PCCP

Accepted Manuscript

ROYAL SOCIETY OF CHEMISTRY

www.rsc.org/pccp

Hierarchical multi-scale simulations of adhesion at polymer-metal interfaces: Dry and wet conditions

Gokhan Kacar [a,*], *Elias A.J.F. Peters* [a], *Leendert G.J. van der Ven* [a,b], *Gijsbertus de With* [a,*]

[a] Laboratory of Materials and Interface Chemistry, Department of Chemical Engineering and Chemistry, Eindhoven University of Technology, Eindhoven, The Netherlands.

[b] AkzoNobel Automotive & Aerospace Coatings, Sassenheim, The Netherlands.

* E-mail: g.dewith@tue.nl, Tel.: +31-40-247-4947

* E-mail: g.kacar@tue.nl, Tel.: +31-40-247-8064

ABSTRACT

We performed hierarchical multi-scale simulations to study the adhesion properties of various epoxy-aluminium interfaces in the absence and presence of water. The epoxies studied differ from each other in their hexagonal ring structures where one contains aromatic and the other aliphatic rings. As aluminium unavoidably is covered with alumina, a cross-linked epoxy structure near an alumina substrate is created and relaxed by performing coarse-grained simulations. To that purpose, we employ a recently developed parameterization method for variable bead sizes. For polymer-metal interactions, a multi-scale parameterization scheme is applied where the relative adsorption of each bead type is quantified. At the mesoscopic scale, the adhesion properties of different epoxy systems are discussed in terms of their interfacial structure and adsorption behavior. To further perform all-atom simulations, the mesoscopic structures are transformed into atomistic coordinates by applying a reverse-mapping procedure. Interface internal energies are quantified and the simulation results observed at different scales are compared with each other as well as with the available experimental data. The good agreement between observations from simulations and experiments show the usefulness of such an approach to better understand polymer-metal oxide adhesion.

INTRODUCTION

Polymeric coating materials are extensively used to protect metallic parts from dust, moisture, or corrosion for a wide range of industrial applications. Moreover, polymers are often used for bonding metals parts, for example, in aircraft construction epoxy polymers are frequently used as an adhesive material for aluminum due to their properties like good chemical resistance, strong adhesion, and good mechanical performance [1, 2]. The adhesion between epoxy and aluminum is important for the reliability of those interfaces. Better adhesion means a longer-life time of products and various methods have been proposed to increase the adhesion of epoxies to aluminum substrates or actually to the inevitably present oxide on the metal surface (alumina) [3, 4]. Moreover, it is well-known that the presence of external agents such as water, adversely influences the adhesion strength at the epoxy-alumina interfaces [5-7]. In an attempt to reduce the negative influence of water on adhesion, recently in our group, various epoxy-amine systems containing aromatic and aliphatic rings were developed [8]. In that work, it was observed that the epoxy with aliphatic groups has better adhesion to the aluminum in the presence of water than the one having aromatic groups. In this paper, we strive to investigate the main factors causing this unexpected adhesion difference. As adhesion is mainly characterized by the molecular level interactions and structure, a detailed study at this scale is inevitably necessary for a proper understanding of the adhesive properties.

As information on the molecular scale origin of the interface structure and properties is difficult to extract directly from experiments, performing molecular simulations is a widely employed alternative. Computational modeling of polymers is somewhat complicated as it includes many aspects occurring at different length scales. At the atomistic scale, vibrations mostly happen at time and length scales in the order of femtoseconds and Ångstroms,

respectively. However, the structural relaxation of polymers usually takes place at much longer time scales, depending on the molecular weights involved. For the case of polymer-metal interfaces, the combination of these fast and slow dynamics lead to the formation of the interfacial structure. Therefore, our scale of interest in this paper is at the intermediate (mesoscopic) and atomistic (microscopic) scale.

In this work, we aim at building a multi-scale simulation scheme to model and study the origins of molecular adhesion of an experimentally studied epoxy-aluminium system. Our multi-scale procedure is two-fold and consists of coarse-grained and atomistic simulations. The first step of our multi-scale attempt is to create a cross-linked polymer structure by using mesoscopic (or coarse-grained) simulations. Since reaching the intrinsic time and length scales necessary for the equilibration of a cross-linked polymer is relatively long, large coarse-grained simulations are frequently employed [9-12]. In this work, we use a mesoscopic simulation method, namely Dissipative Particle Dynamics (DPD) [13], developed as an alternative for methods such as lattice-gas [14] or lattice-Boltzmann simulations [15] and initially applied to model fluids [16]. Later Groot and Warren proposed a parameterization [17] by mapping the model to Flory-Huggins theory [18] thereby extending the model to simulate polymers. This mapping made it possible to obtain DPD parameters from experimental thermodynamic quantities such as solubilities [17, 19]. The abundant availability of such data renders DPD a frequently applied method to study the experimental polymeric systems, either in bulk or near solid surfaces [20-34].

The generic application of DPD to study polymers requires coarse-graining of the polymer structure by grouping atoms together and forming larger molecular entities, generally referred to as *beads.* The conventional DPD parameterization is limited to beads having similar volumes [17]. This has been a severe restriction in the coarse-graining procedure

of experimentally studied polymers. The main reason is that, upon coarse-graining a polymer based on chemical functional groups, significant volume differences might be present, i.e., up to a factor three [35]. This means that a DPD simulation with conventional parameterization results in incorrect local densities, and, as a consequence probably to incorrect morphologies. In an attempt to overcome this limitation, we recently proposed a parameterization procedure that extends the applicability of DPD to different bead sizes [36]. Removing the equal bead volume constraint, makes DPD applicable to a wide range of experimentally relevant polymer systems. Using this parameterization we studied the cross-linking properties and the resulting mesoscopic structure of a cross-linked epoxy [35]. To describe adhesion, it is also essential to correctly model the interactions between polymer and solid surfaces for the systems we consider. Until recently, there has been no parameterization procedure established for such interactions taking into account their intrinsic chemical nature. To that purpose, we reported a multi-scale simulation approach to quantify the mesoscopic DPD parameters between a polymer and a metal or metal-oxide surface [37]. As aluminium unavoidably is covered with oxide, an alumina surface is used to represent the interface. This approach was applied to monitor how the molecular structure of an epoxy was created near an alumina surface.

In this work, we make use of the approaches reported in the previous studies to investigate the adhesive properties of various epoxy-amine systems on aluminium. To determine the adhesive properties at the interface, we combine different length scales. The epoxy structure generated at mesoscopic scale provides us with the initial, but crucial first step towards computing the properties. As a second step, we perform atomistic molecular dynamics (MD) simulations on the atomistic structure derived from the mesoscopic coordinates. The transformation of the mesoscopic structure to the atomistic one can be made by one of the reverse-mapping algorithms [23, 38-43]. Having such a bridge between mesoscopic

and atomistic scales is proven to be an effective tool to proceed for further analysis of the nanoscopic structure [44, 45].

The paper is organized as follows: First, we study the adhesion properties of the epoxies containing either aromatic or aliphatic rings with alumina by discussing the mesoscopic interface structure. Moreover, interface internal energies of these two systems are quantified. In the next section, we consider wet conditions by including water and investigating its effect on the adhesive properties. Finally, we compare the results of the simulations with the available experimental findings.

MATERIALS

Chemical structures and coarse-graining

The epoxies simulated in this paper possess different ring structures: Epikote 828 contains aromatic rings, whereas Eponex 1510 contains aliphatic rings [8]. The epoxies are usually mixed with an amine cross-linker for curing, which is in our case, Jeffamine EDR-148, a polyether amine. To perform the mesoscopic simulations, these chemical structures are coarse-grained in proper chemical functional units. In Fig. 1, the structures and the coarse-grained beads are schematically depicted. The functionality for each functional group is different. Jeffamine contains two primary amine end-groups which makes the molecule four functional. The functionality of the epoxide resin is two. Hence, in a stoichiometric mixture with stoichiometric ratio, the Jeffamine-epoxy molar ratio is 1:2.

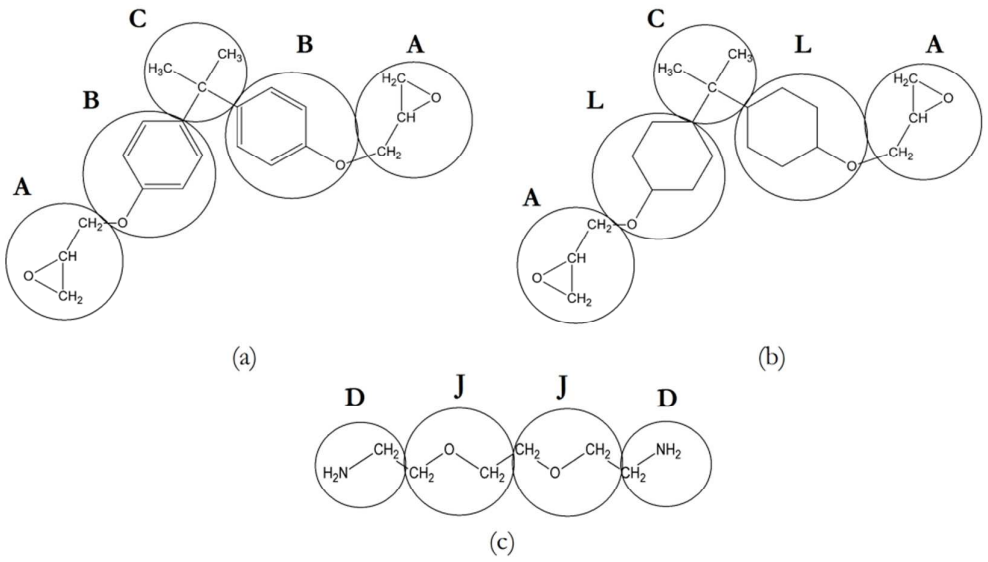

Figure 1. Chemical structures and partitioning in functional groups for the identification of coarse-grained beads for (a) Epikote 828, (b) Eponex 1510, and (c) Jeffamine EDR-148.

The reacting groups that form cross-links correspond to A and D. The cross-linking reactions are based on creating covalent bonds between cross-linking beads if their separation is smaller than a pre-defined distance, 0.3 r_{DPD} in this case. This is the same procedure we used in our previous paper [35, 37] where we showed that the value used for this criterion only affects the dynamics and not the end-structure. Moreover, we recently showed that the nature of the cross-link criterion, i.e., using either a step function or a somewhat more sophisticated continuous function, also does not affect the results significantly [46]. Upon reaction of the cross-linking bead pairs, the chemical nature of the reacting beads change, which means they evolve into new bead types. These reactions read at the meso-scale as: A + D → A′ + D′ and A + D′ → A′ + D″. The chemical structures of these newly formed beads (A′, D′, D″) are shown in Fig. 2.

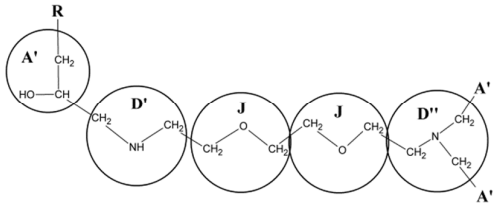

Figure 2. Coarse-grained bead representations illustrating the new bead types formed as a result of the change in internal chemical structure upon cross-linking. The '-R' group indicates the rest of the epoxies.

The epoxies interact with α-alumina (α-Al_2O_3) substrate exhibiting the <0001> surface which is thermodynamically the most stable surface [47, 48]. Alumina has a distorted hexagonal close packed structure with space group $R\bar{3}c$. The structural details of how the alumina structure is modeled at mesoscopic and atomistic scales are given in following sections.

COMPUTATIONAL METHODS AND DETAILS

Dissipative Particle Dynamics (DPD)

DPD is a coarse-grained simulation method, which has a soft, repulsive non-bonded potential with effective interactions. Due to the repulsive nature of the potential, the overall structure is kept intact with an applied pressure. The pressure in simulations is calculated from the forces as a result of the pair interactions. The total force between beads i and j is sum of three components: $\vec{f}_{ij} = \vec{f}_{ij}^{\,\mathrm{C}} + \vec{f}_{ij}^{\,\mathrm{D}} + \vec{f}_{ij}^{\,\mathrm{R}}$, where $\vec{f}_{ij}^{\,\mathrm{C}}$ represents the conservative, $\vec{f}_{ij}^{\,\mathrm{D}}$ the dissipative, and $\vec{f}_{ij}^{\,\mathrm{R}}$ the random force, respectively. The dissipative and random forces are coupled to each other by a fluctuation-dissipation relation and characterize the dynamics of thermostating the system [49]. The functional forms are, respectively,

$$\vec{f}_{ij}^{\,\mathrm{D}} = -\gamma w^{\mathrm{D}}(r_{ij})(\vec{r}_{ij}v_{ij})\vec{r}_{ij} \quad \text{and} \quad \vec{f}_{ij}^{\,\mathrm{R}} = -\sigma w^{\mathrm{R}}(r_{ij})\theta_{ij}\vec{r}_{ij}. \qquad (1)$$

In Eq. 1, γ and σ are the amplitudes of the dissipation and the repulsion, w^D and w^R are weight functions dependent on the position r, while θ_{ij} is a noise term fluctuating with Gaussian statistics having zero mean, and $v_{ij} = v_i - v_j$, $\vec{r}_{ij} = \boldsymbol{r}_{ij}/|\boldsymbol{r}_{ij}|, \boldsymbol{r}_{ij} = r_i - r_j$, $r_{ij} = |\boldsymbol{r}_{ij}|$. In our simulations, we use the optimized values as reported by Groot and Warren [17] for those parameters. The functional forms of the weight functions and the amplitudes for the dissipative and random contributions are, respectively

$$\sigma^2 = 2\gamma k_B T \quad \text{and} \quad w^D(r_{ij}) = [w^R(r_{ij})]^2 = \begin{cases} \left(1 - \frac{r_{ij}}{r_{DPD}}\right)^2 & r_{ij} < r_{DPD} \\ 0 & r_{ij} \geq r_{DPD} \end{cases}. \qquad (2)$$

The equilibrium structure is determined by the conservative forces. All the forces act in a pair-wise fashion such that the momentum is conserved. This results in the proper hydrodynamic behavior at larger time and length scales [16].

The total conservative potential of DPD is a sum of bonded and the non-bonded terms. We use stretch and bending potentials for the bonded terms [50]. The parameters used in our simulations for the bonded interactions are given in the Supporting Information.

The non-bonded potential between two beads i and j with interaction parameter a_{ij} is soft, short-ranged, and purely repulsive and follows the expression

$$V_{DPD,ij}(r_{ij}) = \begin{cases} \frac{a_{ij}}{2}\left(1 - \frac{r_{ij}}{r_{DPD}}\right)^2 & r_{ij} < r_{DPD} \\ 0 & r_{ij} \geq r_{DPD} \end{cases}. \qquad (3)$$

In this paper, we take the dimension of the a_{ij} as energy. However, it is sometimes interpreted as having the dimension force. Therefore in some expressions, the symbol r_{DPD} explicitly appears while it is absent in similar expressions in other publications. Note that r_{DPD} defines the interaction cut-off for non-bonded beads and is the same for all beads [35].

Generally, the repulsive DPD interactions between beads are mapped from Flory-Huggins mean field theory onto DPD [17] via

$$\Delta a_{ij} = 3.51\chi_{ij}k_{\mathrm{B}}T, \Delta a_{ij} = a_{ij} - \hat{a}_{ij} \text{ at } \rho r_{\mathrm{DPD}}^3 = 3 \quad (4)$$

where $\hat{a}_{ij}$ represents the neutral repulsion parameter defining the mixing of beads i and j when there is no excess repulsion, ρ is the dimensionless number density, and χ_{ij} the Flory-Huggins parameter. The latter is directly related to solubility parameter δ of beads which characterizes their mixing or demixing nature: $\chi_{ij} = V_{\mathrm{bead}}(\delta_i - \delta_j)^2/k_{\mathrm{B}}T$. The parameter V_{bead} corresponds to the molar volume of a bead, and in our case is calculated by the weighted average of the pure species volumes [35]. The average bead volume V_{bead} is directly related to the r_{DPD} via $\rho r_{\mathrm{DPD}}^3 = 3$, therefore r_{DPD} = 7.15 Å.

The Groot and Warren mapping applies to equal like-like interactions $\hat{a}_{ij} = a_{ii} = a_{jj}$. However, as mentioned in the introduction, the coarse-graining of epoxy beads is based on the proper partitioning of the chemical groups which results in different bead volumes [35]. The proposed extension to be able to apply DPD to polymers that have different bead volumes [36] is briefly described below.

The identification of like-like parameters a_{ii} originates from the idea that there is mechanical equilibrium between different beads having different experimental pure liquid volumes. This equilibrium ensures that a_{ii} will be different for each bead type and its associated volume is correct when a system is phase-separated. From the DPD equation-of-state (EoS), this was found as [36]

$$a_{ii} = \frac{p - \rho_{i,\mathrm{pure}}k_{\mathrm{B}}T}{\alpha\rho_{i,\mathrm{pure}}^2 r_{\mathrm{DPD}}^3} \quad (5)$$

In Eq. 5, p is the set pressure, ρ is the pure-liquid number density, and α is a constant in the DPD EoS, equal to 0.101 for total number densities higher than 3 [17].

The form of pair-wise interactions a_{ij} between beads having different volumes is derived from a scaling relationship introducing a front factor to the Flory-Huggins χ_{ij} parameter [36] with a neutral interaction parameter $\hat{a}_{ij} = \sqrt{a_{ii}a_{jj}}$. The relation reads

$$a_{ij} = \hat{a}_{ij} + \frac{p}{0.0454(a_{ii}\rho_{i,\text{pure}} + a_{jj}\rho_{j,\text{pure}})}\chi_{ij}k_{\text{B}}T. \quad (6)$$

The DPD interaction parameters between the polymer and metal-oxide beads are derived by quantifying the preferential adsorption for each polymeric bead type at the alumina interface. The surface excess Γ [51] parameter is calculated to characterize the adsorption [37]. The procedure is based on matching Γ, as calculated from atomistic MD, to DPD. The relation for Γ reads

$$\Gamma = \int_{-\infty}^{L_s} \rho(z)dz + \int_{L_s}^{\infty} (\rho(z) - \rho_{\text{bulk}})dz \quad (7)$$

where, $\rho(z)$ and ρ_{bulk} are the bead number densities in the dimension perpendicular to the surface plane and in the bulk-phase, respectively and L_s represents the location of the surface.

Details of DPD simulations

We construct two simulation boxes that contain Epikote-Jeffamine and Eponex-Jeffamine, respectively. The parts consisting of polymer and alumina are glued together to create an organic-inorganic interface oriented along the *xy*-plane. The polymer part includes 10000 Epikote (or Eponex) chains mixed with 5000 Jeffamine chains. This corresponds to a total number of 100258 beads. The beads of the metal-oxide substrate are packed in a face-

centered-cubic structure with a number density of 15 to prevent penetration of polymer beads into the substrate [37]. The simulation box dimensions are x = 25 r_{DPD}, y = 25 r_{DPD} and z = 39.8 r_{DPD} providing a total number density of 3 r_{DPD}^{-3}. The substrate thickness is equal to 2.42 r_{DPD}.

We run simulations in an *NPT* ensemble and control the pressure only in the direction perpendicular to interface. The coordinates of the metal-oxide substrate beads are held fixed during the simulations. Therefore the pressure is calculated only in the epoxy layer excluding the metal bead contribution. The pressure value in simulations is set as p = 38.5 r_{DPD}^{-3} in order to give a correct order of magnitude of overall compressibility [36]. The total number of simulation steps is $2 \cdot 10^6$ with the first $1 \cdot 10^6$ steps for equilibration and the rest for data collection. The cross-linking reactions are switched on after the equilibration run is finished. The time step in the simulations is set as Δt = 0.02 t_{DPD}. Periodic boundary conditions are employed in all dimensions. We used the LAMMPS MD simulator [52, 53] to perform the DPD simulations.

Details of atomistic MD simulations

To perform atomistic simulations, we use a reverse-mapping algorithm built in-house which creates the atomistic structure of the polymer from the meso-scale coordinates [42, 43]. The reverse-mapping algorithm is composed of three steps: 1) Insertion of the atomistic templates (molecular units corresponding to beads), 2) rotation shortening the distances between consecutive templates, and 3) energy minimization. The input structure for the reverse-mapping procedure is obtained from mesoscopic simulations performed on a smaller box than highlighted in the previous section. If the reverse-mapping procedure is applied to the same box, this would correspond to approximately 620,000 atoms. This is too large to simulate at reasonable computational times. The box dimensions used therefore are x = 7.98

r_{DPD}, y = 8.07 r_{DPD} and z = 12.15 r_{DPD}, constituting a total of 3600 beads. These box lengths are sufficiently large so that no persistent density fluctuations might result from the periodic boundary conditions. When the DPD coordinates are scaled with the physical length scale (that is, 7.15 Å [35]), the initial dimensions become 57.1 Å, 57.7 Å, and 86.7 Å in *xyz* with 18600 atoms in the epoxy layer.

The alumina crystal structure is obtained from the Materials Studio [54] structural database. The fine-grained polymer structure is combined with the alumina structure such that the interface lies in the *xy*-plane. Atomistic simulations are performed with the LAMMPS [52, 53] software by using the Polymer Consistent Force Field (PCFF) [55] which is parameterized for various organic and inorganic materials and is capable of predicting material properties of a bulk cross-linked epoxy in agreement with the experimental reports [43]. Prior to the simulations, an energy minimization step, using a combination of Newton-Raphson and conjugate gradient algorithms, is performed for the epoxy layer while the alumina atoms are held fixed at their positions. After the energy minimization, atomistic simulations are performed at *NPT* conditions. Similar to the coarse-grained simulations, we control the pressure perpendicular to the epoxy layer excluding the contribution of metal atoms. We run the simulations with 0.1 fs timestep for a total of 100 ps. Later, simulations are restarted with 1 fs timestep for a total of 1 ns. The cut-off radius used for non-bonded Lennard-Jones interactions is 10 Å while the electrostatic Coulomb interactions are handled by the particle-mesh Ewald [56] summation. The temperature is set as room temperature using the Nosé-Hoover thermostat [57, 58] while pressure control is performed by the Parinello-Rahman [59] barostat, set at pressure 1 atm.

Consideration of water in simulations

The effect of water is studied by means of mesoscopic and atomistic scale simulations. The interaction parameters to simulate water interactions with itself and with the rest of the beads are given in the Supporting Information.

In the experimental practice, the epoxy is immersed in water after the polymer is cured and the effect of water on the adhesion strength is studied. In order to mimic the experimental procedure [8], we follow the same sequence of events in our simulations. This means that we first obtain the cross-linked epoxy structure at the mesoscopic scale and then create water beads with random coordinates inside the bulk polymer. The wet epoxy system is run for an extra of $1 \cdot 10^6$ DPD steps to relax the structure. The water molar fraction in the polymer is taken as the experimental values, corresponding to 3.82 % in Epikote and 0.13 % in Eponex [8]. For the mesoscopic simulations, we simulated a large box with 27759 and 1006 water beads, respectively. After reverse-mapping, similarly to the previous consideration, we simulate a smaller box for computational efficiency. The wet epoxy contains 833 water beads for the Epikote and 30 water beads for the Eponex polymer.

Quantification of interface internal energies

Quantification of interface internal energies requires performing MD simulations. To that purpose, we decorated the coarse-grained coordinates with the atomistic detail *via* the reverse-mapping procedure, as detailed in reference [42]. We discuss the adhesion properties of the epoxy-alumina interfaces in terms of the calculated interface internal energies. This quantity has been used in literature to discuss the strength of adhesion for different type of interfaces [48, 60, 61]. The interface internal energy is the binding (or potential) energy associated with the polymer-metal interaction and characterizes the energy required to break all the

interactions between the epoxy and alumina. It provides how stable an interface is, is directly proportional to the strength of adhesion at the interface [62], and described by

$$E_{\text{interface}} = E_{\text{total}} - \left(E_{\text{epoxy}} + E_{\text{alumina}}\right) \quad (8)$$

where E_{total} is the total energy of the epoxy and alumina, E_{epoxy} is the total energy of epoxy without alumina, and E_{alumina} is the total energy of the alumina crystal excluding the epoxy layer. A negative value indicates a favorable interaction between the polymer and substrate.

We should note here that Eq. 8 provides the internal energy as the interface internal energy. This is different from the 'work of adhesion' (or interface Gibbs energy) which is the energy necessary to create the polymer-metal interface at constant P and T. The calculation of the Gibbs energy can be done by various procedures such as thermodynamic integration at a particular temperature or by temperature integration of Gibbs energies computed at different temperatures [63]. Both procedures require performing extensive simulations. In this work we proceed to discuss our results by means of interface internal energies, as this quantity sufficiently characterizes the strength of interactions present at the interface.

To satisfy that the polymer only feels a single surface, we extend the simulation box in the dimension perpendicular to the interface by placing 30 Å vacuum on top of the polymer layer. The interface internal energy $E_{\text{interface}}$ is calculated after we performed an additional 2 ns run subsequent to simulations as described in previous sections.

RESULTS AND DISCUSSION

Adhesion of dry epoxies to alumina

We first discuss the adhesion properties of the dry epoxy polymer on the alumina substrate, as deduced from their mesoscopic structures for the cases that cross-linking is present or not.

Analyzing *non*-cross-linked interfacial structures will give insight in the molecular origin leading to the formation of the interfacial structures. We examine the density profiles, the density fluctuations and width of the interface to provide insight on the relative adsorptions of functional groups on the substrate.

The non-cross-linked density profiles are depicted in Fig. 3. The epoxy (bead A) is observed to be the nearest to the alumina substrate for both of systems, but it is slightly closer in Epikote due to the non-bonded interactions of type B (aromatic ring) and type L (aliphatic ring) with the alumina. The bonded interactions of these groups with the epoxy groups (bead A) are also influencing the interfacial structures. In other words, considering that bead L is more repulsive (see Table S1) to alumina, it drags the epoxy group into the bulk region in Eponex.

The concentration of Jeffamine beads (D and J) at the interface is higher for Eponex. They can reach more easily the interface as a result of their less repulsive interactions with alumina. Moreover, bead containing the aliphatic ring, the L bead for Eponex, has a sharper profile than its counterpart in Epikote, bead B. This is related to the depletion observed at around 3.5 r_{DPD} and the aliphatic beads play a minor role as a barrier preventing the migration of other beads towards the interface.

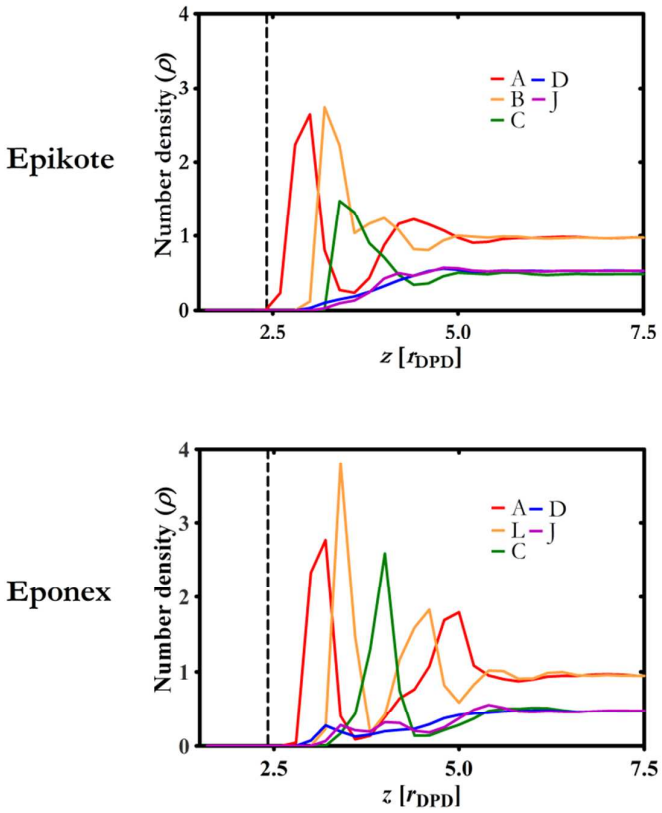

Figure 3. The density profiles of the *non*-cross-linked Epikote-Jeffamine and Eponex-Jeffamine systems near the alumina interface. The profiles are shown until 7.5 r_{DPD} in the direction perpendicular to the interface as at this distance the bulk density is reached. The vertical dashed line indicates the location of the alumina substrate.

Density profiles provide crucial information to understand the adsorption behavior of beads. To further comment on the adhesion of the two interfaces, we compute and compare the surface excess Γ-values, which quantifies how much a particular bead type is adsorbed as compared to the others. The calculation is similar to the parameterization of polymer-alumina interactions. The results indicate whether the system is more or less favored by the alumina and are reported in Table 1. Higher value of Γ indicates more adsorption.

Table 1. The surface excess values computed for different beads in *non*-cross-linked Epikote-Jeffamine and Eponex-Jeffamine systems. The integration in Eq. 7 is taken from the location of the surface (z = 2.42 r_{DPD}) until the middle of the simulation box. The total amount is computed from the average density of beads. The dashes show that those bead types are not present in the epoxy system.

Γ [r_{DPD}]	Epikote-Jeffamine	Eponex-Jeffamine
A	0.0893	0.0863
B	0.0761	–
L	–	0.0847
C	0.0390	0.0207
D	–0.6256	–0.8939
J	–0.6349	–0.8874
Total	–1.0561	–1.5896

Comparing the same bead types in different systems reveals the differences in the density profiles. A significant difference is observed for the Jeffamine beads (D and J) in the two systems favoring the adsorption of Epikote. The aliphatic ring (bead L) adheres more than its counterpart in Epikote. The Γ-values for the epoxy functional groups (bead A) are not significantly different from each other but slightly in favor of Epikote. The bottom row quantifies the total amount of adsorption signifying that the total adsorption of Epikote is higher than the Eponex. This is in line with the interaction parameters of the ring structures and the alumina, for which the aromatic ring is less repulsive than the aliphatic ring.

The interfacial structure changes upon cross-linking. The transition of beads to different (and new) types alters the interactions, and ultimately, their concentration near the alumina interface. A clear example is seen in Fig. 4 where for both epoxies once reacted amine groups (bead D) have almost zero concentration all over the simulation box. In addition, a surplus of unreacted epoxy functional groups (bead A) exists near alumina, although they are nearly

absent in the bulk. This is possibly caused by the preferential formation of cross-links in the bulk rather than near the alumina at the initial stage of reaction. A similar effect can be found in reference [37]. A small concentration of unreacted cross-linking beads in the bulk indicates that a high cross-link conversion is reached. For both systems, the computed cross-link conversion values are about 0.92.

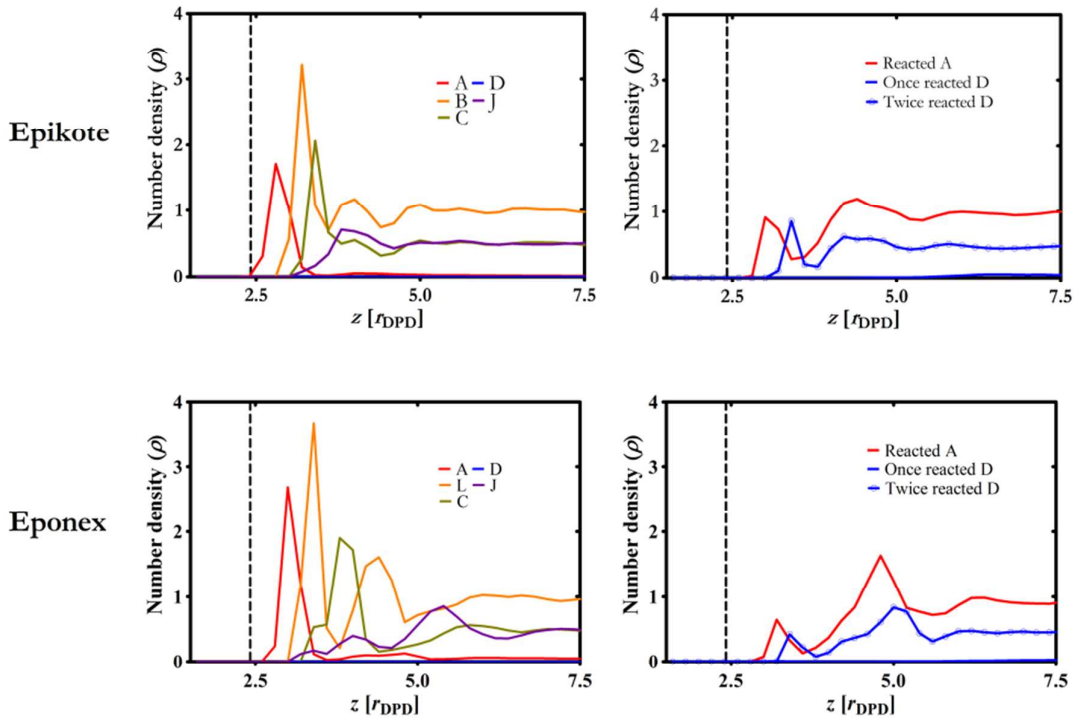

Figure 4. The density profiles of the cross-linked Epikote-Jeffamine and Eponex-Jeffamine systems near the alumina interface. The profiles are shown until 7.5 r_{DPD} in the direction perpendicular to the interface as at this distance the bulk density is reached. The vertical dashed line indicates the location of the alumina substrate. Note that in the right figures for both epoxies once reacted amine groups (bead D) have almost zero concentration all over the simulation box.

Similar to the *non*-cross-linked epoxies, we calculated the surface excess for each bead type and the total for the cross-linked materials. Table 2 depicts the adsorbed amount of a specific bead type near alumina for the cross-linked epoxies. The adsorption of unreacted epoxy functional groups is higher for Eponex than for Epikote. Upon cross-linking the epoxy functional group results in bead type A′ which, in line with its interaction parameter, is concentrated near the interface of Epikote. A similar comment can be made for the reacted amine groups. On the whole, Epikote shows more adsorption to the alumina surface than the Eponex.

Table 2. The surface excess values computed for different beads in cross-linked Epikote-Jeffamine and Eponex-Jeffamine systems. The integration in Eq. 7 is taken from the location of the surface (z = 2.42 r_{DPD}) until the middle of the simulation box. The total is computed from the average density of beads. The dashes show that those bead types are not present in the corresponding systems.

$\Gamma[r_{DPD}]$	Epikote-Jeffamine	Eponex-Jeffamine
A	0.6703	0.9797
B	–2.2795	–
L	–	–2.2322
C	–1.1420	–1.1128
D	–0.0297	–0.0045
J	–1.7002	–1.9168
A′	–2.9078	–3.1769
D′	–0.3575	–0.5946
D″	–1.3489	–1.3505
Total	–9.0953	–9.4086

In addition to the analysis of the mesoscopic structures, we performed atomistic simulations for further quantification of the adhesion properties and calculated the interface internal energies of the epoxy-alumina interfaces.

To illustrate the relative adhesion strength of two epoxies, we report in Table 3, the interface internal energies E per unit area A, as computed from the atomistic MD simulations. The cross-link conversions X are also given to demonstrate that all the systems have similar degree of cross-linking. The minus sign in front of the interface internal energies indicates that the epoxies are favored by the alumina.

Table 3 shows that the adhesion of two epoxies does not differ too much, but is slightly in favor of Epikote, i.e., the epoxy which contains the aromatic ring, as also revealed by the surface excess obtained from the mesoscopic simulations.

Table 3. Interface internal energies are computed from atomistic simulations for the epoxies. The computational errors are smaller than 0.001 J/m^2.

Mixture	X	$E_{\text{interface}}/\text{A}$ (J/m^2)
Epikote-Jeffamine	0.92	–0.663
Eponex-Jeffamine	0.91	–0.609

Experimental measurements illustrate that the average value of the adhesion strength of Eponex is slightly higher than for Epikote [8], in contrast to our simulation results for the adhesion energies. Note that experimentally strength is measured while here energy is discussed. The link between these quantities is provided by the critical flaw size, which is not necessarily the same for both epoxies. Moreover, the standard deviations in experimental measurements are relatively large as they reflect the flaw size distribution [62].

Effect of water on epoxy-alumina adhesion

The experimental work of Meis *et* al. [8] further demonstrated that the differences in adhesion strengths become more pronounced when the epoxies are tested in wet conditions. Therefore,

we also considered the effect of water on the interface structure and energies. We first discuss the influence of water on the meso-scale structure of the interface and the bulk. The DPD parameters indicate that water has a very high repulsion with the epoxy beads and attraction with the alumina (see Table S1). Therefore, it is energetically favored that the water beads stay at the interface. As a result of the trade-off of these interactions, in Fig. 5, water is observed as spheres in the bulk, and as a mixture of spheres and as a thin layer at the interface.

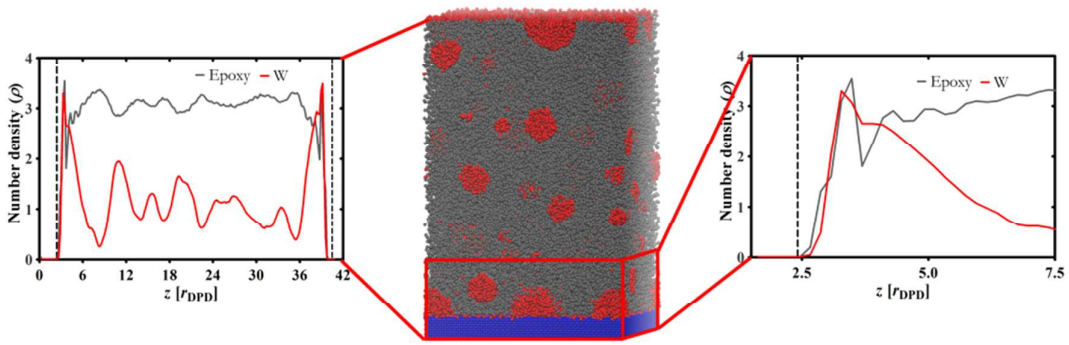

(a)

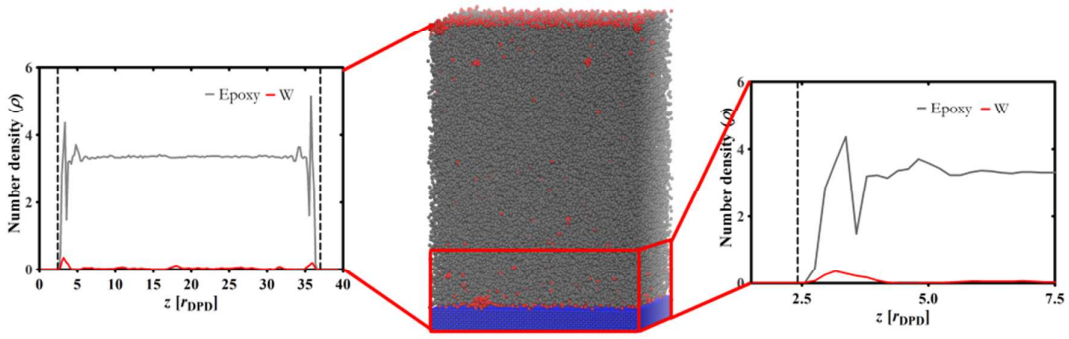

(b)

Figure 5. Density profiles (left and right) of the cross-linked epoxies (gray) near alumina in the presence of water (red) in (a) Epikote-Jeffamine, (b) Eponex-Jeffamine. The number density of epoxies are calculated by taking the average number of beads irrespective of their

type. The middle picture is a snapshot taken at the end of the simulation. The vertical dashed line indicates the location of the alumina substrate.

The total water content is another factor influencing the structure of water in polymer. If the water concentration is low, it may prefer to segregate to the interface as the critical concentration to form water clusters cannot be reached. In contrast, if the water content is above a certain limit, attractive water-water interactions might result in the formation of water clusters in bulk rather than water beads migrating towards the interface. The water concentration in Epikote is much higher than in Eponex. Despite the fact that the water concentration in Eponex is small, a small portion of water clusters is trapped in the bulk due to the cross-linked nature of polymer as the network prevents these clusters to escape towards the interface.

Next, the relative adsorption of the epoxies are studied as influenced by the presence of water. The total amount of adsorption presented in Table 4 indicate that adsorption of the Eponex is better than for the Epikote. The extent of the adsorption difference is large, about 22 %, while for the dry epoxy the difference was only 3 %. A negative influence of water on the adsorption of epoxy to alumina is observed. Comparing the individual beads, the largest difference is observed for the unreacted epoxy group (bead A), and in favor of the Eponex. This is followed by the once and twice reacted amine groups (beads D′ and D″, respectively), and bead J. The rest of the beads show minor differences in two epoxies. Water adsorption is clearly higher in Epikote. As a result of the presence of water at the interface, epoxies are observed to delaminate from alumina.

Table 4. The surface excess values computed for different beads in the cross-linked Epikote-Jeffamine and Eponex-Jeffamine systems. The integration in Eq. 7 is taken from the location of the surface (z = 2.42 r_{DPD}) until the middle of the simulation box. The total is computed only from the average density of epoxy beads with the water beads are excluded. The dashes show that those bead types are not present in the corresponding systems. W indicates the water bead.

$\Gamma[r_{DPD}]$	Epikote-Jeffamine **+ Water**	Eponex-Jeffamine **+ Water**
A	0.7393	1.1634
B	–0.3211	–
L	–	0.0622
C	–0.1584	0.0362
D	–0.0019	0.0000
J	–0.7039	–0.9425
A′	–1.0415	–1.1046
D′	–0.3310	–0.7084
D″	–0.4004	–0.2429
W	2.0914	0.1312
Total	–2.2187	–1.7365

Making a direct comparison to the dry epoxy case is difficult as the water concentration introduce inhomogeneities which significantly affects the structure at the interface. In order to meaningfully compare with the dry epoxies, in the next section, we perform atomistic simulations on the wet epoxies.

The calculated interface internal energies illustrate a major decrease in adhesion of Epikote to alumina as shown in Table 5. The separation of the epoxy polymer from alumina significantly decreases the interface internal energy of Epikote. The more water accumulated at the interface, the more delamination occurs which lowers the adhesion. Comparing with

the interface internal energies of dry epoxies (see Table 3), there is no major change for Eponex. However, the interface internal energy is decreased almost half for Epikote.

Table 5. Interface internal energies computed from atomistic simulations of the epoxies. The computational errors for all epoxies are smaller than 0.001 J/m^2. Cross-link conversion values X for each epoxy are given.

Mixture	X	$E_{\text{interface}}/A$ (J/m^2)
Epikote-Jeffamine + **Water**	0.92	–0.347
Eponex-Jeffamine + **Water**	0.91	–0.626

Overall, the simulation results correctly represent the qualitative experimental conclusions in dry and wet conditions. On the other hand, experimental data report the interfacial strength values obtained from pull-off tests, whereas we estimate the interface internal energies between the epoxies and the alumina. Therefore, a direct comparison of simulation results with the experimental measurements is not straightforward. During the pull-off tests the material undergoes deformation until fracture occurs. The measured quantity is then the stress at the fracture. In order to perform a direct comparison between the experimental data and the computational values, Griffith's criterion [62] could be used. This criterion is based on an 'energy approach' to continuum fracture, and is valid for substances that are brittle upon fracture. Griffith found that the product $\sigma_f \sqrt{a}$ is related to a materials constant K, where σ_f is the stress at fracture, and a is the flaw size. The Griffith theory indicates that the constant K is directly related to the elastic modulus E of the material, Poisson's ratio v, and the interface internal energy γ with the expression for plane strain and monolithic materials reading $K = \sqrt{2E\gamma/\pi(1-v^2)}$. But we have to bear in mind that for the

experiments, we do not know explicitly the flaw size *a*, and additionally, we have a bi-material interface, so that the exact expressions are more complex. Moreover in reality, the epoxy-alumina interface might involve chemical bonds but we only model the non-bonded interactions between the epoxy and alumina. Finally, the surface morphology of alumina in reality contains irregularities such as kinks, steps, defects, hydroxyl groups, impurities, etc., which could alter the strength of adhesion significantly. For a proper comparison, these effects should be taken into account.

CONCLUSIONS

In this paper we simulate, in dry and wet conditions, two epoxies interacting with alumina to reveal the adhesion differences and to obtain the structural and energetic properties of the interface. The epoxies differ from each other solely by their ring structures with one having an aromatic and the other an aliphatic ring. The motivation for the simulations arose from the (counter-intuitive) conclusion of the experimental work reporting that the epoxy which contains the aliphatic rings has in wet conditions a better adhesion to the alumina than the epoxy with the aromatic rings. By using molecular simulations at different length scales, we monitored and analyzed the underlying structural and energetic factors that influence the adhesion differences of epoxy to alumina with and without the presence of water.

The procedure we follow is a multi-scale approach. First, we perform mesoscopic DPD simulations to create the cross-linked epoxies since obtaining the time scales necessary to reach high cross-link conversions is not feasible with all-atom simulations. We model the epoxies with the parameters calculated *via* a generalized DPD parameterization approach considering variable bead volumes. Moreover, we compute the polymer-alumina DPD interactions from a dual-scale simulation approach. At mesoscopic scale, we analyze the structure of epoxies at the interface to monitor the adhesion behavior. As a result, we find

that the epoxy with the aromatic rings is slightly more adsorbed to the alumina in dry conditions. In contrast, we observe significantly more adsorption for the aliphatic epoxy in wet conditions.

To estimate the physical adhesion at the interfaces, we perform atomistic MD simulations for two epoxies. The atomistic coordinates are derived from the mesoscopic coordinates *via* a reverse-mapping approach. We calculate the interaction with the interfaces and find that the results at different scales agree with each other. That is, for the epoxy that is adsorbed more, we find a higher degree of adsorption (DPD) and a higher interface internal energy (MD). The adhesion level for the dry case is similar for both epoxies, but when water is present, adhesion of Epikote decreases significantly. The interaction of water with the polymer is repulsive and attractive with the alumina. Therefore, water prefers to stay near the alumina. However, water clusters are formed in bulk epoxy as the water molecules are trapped inside the cross-linked network and could not reach the interface. These water clusters are observed to be present in the form of spheres or as a thin layer as a result of the trade-off between water-alumina, water-epoxy and epoxy-alumina interactions. Overall, the amount of water in the polymer-metal(oxide) interface significantly alters the interfacial structure by introducing inhomogeneities which eventually results in the loss of adhesion.

In light of the adsorption and adhesion behavior of different epoxies to alumina as quantified by these hierarchical multi-scale simulations, we conclude that the qualitative order of the experimental adhesion strengths is explained successfully, thus providing a clear understanding on the energetic and structural factors playing a role in adhesion differences. The hierarchical multi-scale approach presented in this paper can be extended to study similar interfaces of interest and possibly guiding potential experimental work in this field.

ACKNOWLEDGMENTS

Part of this work is financially supported by the Technology Foundation STW within MuST (Multi Scale Simulation Techniques) framework with project no. 10121. Dr. Niels Meis is thanked for the fruitful discussions on the experimental results.

References

1. S. Lin, H. Shih and F. Mansfeld, *Corros. Sci.*, 1992, **33**, 1331-1349.
2. R. L. Twite and G. P. Bierwagen, *Prog. Org. Coat.*, 1998, **33**, 91-100.
3. C. Bockenheimer, B. Valeske and W. Possart, *Int. J. Adhes. Adhes.*, 2002, **22**, 349-356.
4. J. van den Brand, S. Van Gils, P. C. J. Beentjes, H. Terryn, V. Sivel and J. H. W. de Wit, *Prog. Org. Coat.*, 2004, **51**, 339-350.
5. J. van den Brand, S. Van Gils, H. Terryn, V. G. M. Sivel and J. H. W. de Wit, *Prog. Org. Coat.*, 2004, **51**, 351-364.
6. V. V. Arslanov, *J. Adhesion*, 1994, **44**, 257-269.
7. H. Leidheiser and W. Funke, *J. Oil Colour Chem. As.*, 1987, **70**, 121-132.
8. N. N. A. H. Meis, L. G. J. van der Ven, R. A. T. M. van Benthem and G. de With, *Prog. Org. Coat.*, 2014, **77**, 176-183.
9. P. V. Komarov, Y. T. Chiu, S. M. Chen, P. G. Khalatur and P. Reineker, *Macromolecules*, 2007, **40**, 8104-8113.
10. K. Farah, F. Leroy, F. Muller-Plathe and M. C. Bohm, *J. Phys. Chem. C*, 2011, **115**, 16451-16460.
11. H. Yagyu, Y. Hirai, A. Uesugi, Y. Makino, K. Sugano, T. Tsuchiya and O. Tabata, *Polymer*, 2012, **53**, 4834-4842.
12. H. Liu, M. Li, Z. Y. Lu, Z. G. Zhang, C. C. Sun and T. Cui, *Macromolecules*, 2011, **44**, 8650-8660.
13. P. J. Hoogerbrugge and J. M. V. A. Koelman, *Europhys. Lett.*, 1992, **19**, 155-160.
14. J. P. Rivet and J. P. Bonn, *Lattice Gas Hydrodynamics*, Cambridge University Press, Cambridge, 2001.
15. S. Succi, *The Lattice-Boltzmann Equation for Fluid Dynamics and Beyond*, Oxford University Press, Oxford, 2001.
16. P. Espanol, *Phys. Rev. E*, 1995, **52**, 1734-1742.

17. R. D. Groot and P. B. Warren, *J. Chem. Phys.*, 1997, **107**, 4423-4435.
18. P. J. Flory, *Principles of Polymer Chemistry*, Cornell University Press, Ithaca, New York, 1953.
19. R. D. Groot and K. L. Rabone, *Biophys. J.*, 2001, **81**, 725-736.
20. H. Can, G. Kacar and C. Atilgan, *J. Chem. Phys.*, 2009, **131**.
21. R. D. Groot, T. J. Madden and D. J. Tildesley, *J. Chem. Phys.*, 1999, **110**, 9739-9749.
22. O. A. Guskova and C. Seidel, *Soft Matter*, 2012, **8**, 2833-2843.
23. G. Kacar, C. Atilgan and A. S. Ozen, *J. Phys. Chem. C*, 2010, **114**, 370-382.
24. E. Yildirim, G. Erciyes and M. Yurtsever, *Macromol. Res.*, 2013, **21**, 949-957.
25. E. Yildirim, M. Yurtsever, B. Kenarli and A. L. Demirel, *Macromol. Theor. Simul.*, 2011, **20**, 340-349.
26. R. Pool and P. G. Bolhuis, *Phys. Chem. Chem. Phys.*, 2006, **8**, 941-948.
27. M. Dutt, O. Kuksenok, M. J. Nayhouse, S. R. Little and A. C. Balazs, *Acs Nano*, 2011, **5**, 4769-4782.
28. X. Yong, O. Kuksenok, K. Matyjaszewski and A. C. Balazs, *Nano Lett.*, 2013, **13**, 6269-6274.
29. S. Chen, C. Guo, G. H. Hu, H. Z. Liu, X. F. Liang, J. Wang, J. H. Ma and L. Zheng, *Colloid Polym. Sci.*, 2007, **285**, 1543-1552.
30. J. L. Jones, M. Lal, J. N. Ruddock and N. A. Spenley, *Faraday Discuss.*, 1999, **112**, 129-142.
31. A. Maiti, J. Wescott and P. Kung, *Mol. Simulat.*, 2005, **31**, 143-149.
32. P. Malfreyt and D. J. Tildesley, *Langmuir*, 2000, **16**, 4732-4740.
33. I. V. Pivkin and G. E. Karniadakis, *J. Comput. Phys.*, 2005, **207**, 114-128.
34. J. Servantie and M. Muller, *J. Chem. Phys.*, 2008, **128**.
35. G. Kacar, E. A. J. F. Peters and G. de With, *Soft Matter*, 2013, 5785-5793.
36. G. Kacar, E. A. J. F. Peters and G. de With, *EPL*, 2013, **102**, 40009.
37. G. Kacar, E. A. J. F. Peters and G. de With, *J. Phys. Chem. C*, 2013, **117**, 19038–19047.
38. J. Baschnagel, K. Binder, P. Doruker, A. A. Gusev, O. Hahn, K. Kremer, W. L. Mattice, F. Muller-Plathe, M. Murat, W. Paul, S. Santos, U. W. Suter and V. Tries, *Adv. Polym. Sci.*, 2000, **152**, 41-156.
39. G. Milano and F. Muller-Plathe, *J. Phys. Chem. B*, 2005, **109**, 18609-18619.
40. C. Peter and K. Kremer, *Soft Matter*, 2009, **5**, 4357-4366.
41. G. Santangelo, A. Di Matteo, F. Muller-Plathe and G. Milano, *J. Phys. Chem. B*, 2007, **111**, 2765-2773.

42. G. Kacar, Ph.D. Dissertation, Eindhoven University of Technology, 2014.
43. G. Kacar, E. A. J. F. Peters and G. de With, *Comput. Mater. Sci.*, 2015, DOI: 10.1016/j.commatsci.2015.02.021.
44. T. A. Wassenaar, K. Pluhackova, R. A. Böckmann, S. J. Marrink and D. P. Tieleman, *J. Chem. Th. Comp.*, 2014, **10**, 676-690.
45. T. Spyriouni, C. Tzoumanekas, D. Theodorou, F. Muller-Plathe and G. Milano, *Macromolecules*, 2007, **40**, 3876-3885.
46. H. Makki, K. N. Adema, E. A. Peters, J. Laven, L. G. van der Ven, R. A. van Benthem and G. de With, *Polym. Degr. Stab.*, 2014, **105**, 68-79.
47. J. M. McHale, A. Auroux, A. J. Perrotta and A. Navrotsky, *Science*, 1997, **277**, 788-791.
48. T. Semoto, Y. Tsuji and K. Yoshizawa, *J. Phys. Chem. C*, 2011, **115**, 11701-11708.
49. P. Espanol and P. Warren, *Europhys. Lett.*, 1995, **30**, 191-196.
50. D. Frenkel and B. Smit, *Understanding Molecular Simulation: From Algorithms to Applications*, Academic Press, California, London, 2002.
51. A. G. Goicoehea, *Langmuir*, 2007, **23**, 11656-11663.
52. LAMMPS Molecular Dynamics Simulator, http://lammps.sandia.gov.
53. S. Plimpton, *J. Comput. Phys.*, 1995, **117**, 1-19.
54. Materials Studio, Accelrys Software Inc., San Diego, CA.
55. H. Sun, S. J. Mumby, J. R. Maple and A. T. Hagler, *J. Am. Chem. Soc.*, 1994, **116**, 2978-2987.
56. T. Darden, D. York and L. Pedersen, *J. Chem. Phys.*, 1993, **98**, 10089-10092.
57. W. G. Hoover, *Phys. Rev. A*, 1985, **31**, 1695-1697.
58. S. Nose, *J. Chem. Phys.*, 1984, **81**, 511-519.
59. M. Parrinello and A. Rahman, *J. Appl. Phys.*, 1981, **52**, 7182-7190.
60. S. Kisin, J. B. Vukic, P. G. T. van der Varst, G. de With and C. E. Koning, *Chem. Mater.*, 2007, **19**, 903-907.
61. B. Prathab, V. Subramanian and T. M. Aminabhavi, *Polymer*, 2007, **48**, 409-416.
62. G. de With, *Structure, Deformation, and Integrity of Materials. Volume II: Plasticity, Visco-elasticity, and Fracture*, Wiley-VCH Verlag GmbH & Co. KGaA, Weinheim, 2006.
63. W. F. van Gunsteren, X. Daura and A. E. Mark, *Helv. Chim. Acta*, 2002, **85**, 3113-3129.